Recovery of a Luther-Emery phase in the three-band Hubbard ladder with longer-range hopping

Luhang Yang [1,2,*] Thomas P. Devereaux,[1,3] and Hong-Chen Jiang [1]

[1]*Stanford Institute for Materials and Energy Sciences, SLAC National Accelerator Laboratory, Menlo Park, California 94025, USA*
[2]*Department of Physics, Northeastern University, Boston, Massachusetts 02115, USA*
[3]*Department of Materials Science and Engineering, Stanford University, Stanford, California 94305, USA*

A lightly doped single-band Hubbard model on a two-leg ladder exhibits a Luther-Emery phase, whereas the three-band Hubbard ladder behaves as a Luttinger liquid upon hole doping. To understand this discrepancy, we present a systematic density-matrix renormalization group study of the three-band Hubbard model on two-leg cylinders with further-neighbor particle hoppings. The inclusion of the longer-range hopping is motivated by the studies of the single-band Hubbard model in which the further-neighbor hopping terms are suggested to be crucial for the unconventional superconductivity. When the longer-range hopping parameters are small, the ground state is a Luttinger liquid having mutually commensurate superconducting, charge, and spin density wave correlations. Increasing the longer-range hopping drives a transition into a Luther-Emery phase with quasi-long-ranged superconducting and charge orders but short-ranged spin-spin correlations. By down-folding the three-band Hubbard model into an effective t-t'-J-J' model, we find that in the Luther-Emery phase, both the nearest- and second-neighbor kinetic energies are enhanced due to an effective increase of copper-oxygen hybridization. Amplifying intercell oxygen orbital hopping mirrors the benefits of reducing the charge transfer energy, causing doped holes to favor oxygen orbitals and strengthening superconducting pairing.

I. INTRODUCTION

The three-band Hubbard model, which was first proposed by Emery [1,2], can depict the lattice structure of copper and oxygen orbitals in cuprate superconductors. This model is of particular interest because (1) it takes into account the charge-transfer energy and describes the structure of cuprate materials [3,4] better than the single-band Hubbard model, and (2) it provides geometrically decoupled spin and charge degrees of freedom in some parameter range. These characters make it a potentially suitable candidate that favors the pairing order. Besides, recent studies on the three-band Hubbard ladder suggest the presence of a pair density wave (PDW) ground state [5,6], which is a rare find in the microscopic realization of PDW [7–13].

In the context of high-temperature superconductivity, extensive studies have been conducted on the single-band Hubbard model [14,15]. There are some deep relations between the single-band and three-band Hubbard models: the similarity in the fundamental excitations is illustrated by the Zhang-Rice singlet picture [16]; under certain circumstances, the three-band Hubbard model can be down-folded to an effective single-band Hubbard model or t-J model [17–20], where similar ground state properties have been revealed in recent decades [17,21–25]. The ground state of the single-band Hubbard model at half filling on a two-dimensional square lattice is a Mott insulator with long-range magnetic

order [26,27]. The three-band Hubbard model at half filling also has been found to exhibit AFM order [28,29].

However, discrepancies between these two models are not negligible. Although it has been extensively studied in the context of high-temperature superconductivity, no evidence of PDW has been found in the single-band Hubbard model. More strikingly, the single-band Hubbard ladder exhibits a Luther-Emery phase with dominant superconducting and charge orders upon light doping [30,31], whereas the three-band Hubbard ladder is a Luttinger liquid for the same doping concentrations [5,32].

To understand these discrepancies, we study the three-band Hubbard model with longer-range hopping on a two-leg ladder. The inclusion of the longer-range hopping is motivated by previous studies on the single-band Hubbard model, in which the further-neighbor particle hoppings are essential for superconductivity [14,15,33–38]. We study the ground state properties of the lightly doped three-band Hubbard model on two-leg cylinders of Lieb lattices. The further-neighbor hopping terms we introduce here are the hopping between copper sites in the adjacent cells with coefficients t_{dd}, and the hopping between oxygen sites in the adjacent cells with coefficients t'_{pp}. By tuning the hopping parameters, we get a phase diagram with a Luttinger liquid phase with intertwined PDW, charge density wave (CDW), and spin density wave (SDW) correlations when both hoppings are close to zero, and a Luther-Emery SC phase with d-wave symmetry when these two parameters are greater than a critical value.

The rest of the article is organized as follow: in Sec. II, we describe the model Hamiltonian and illustrate the phase diagram; in Sec. III, we show various ground state
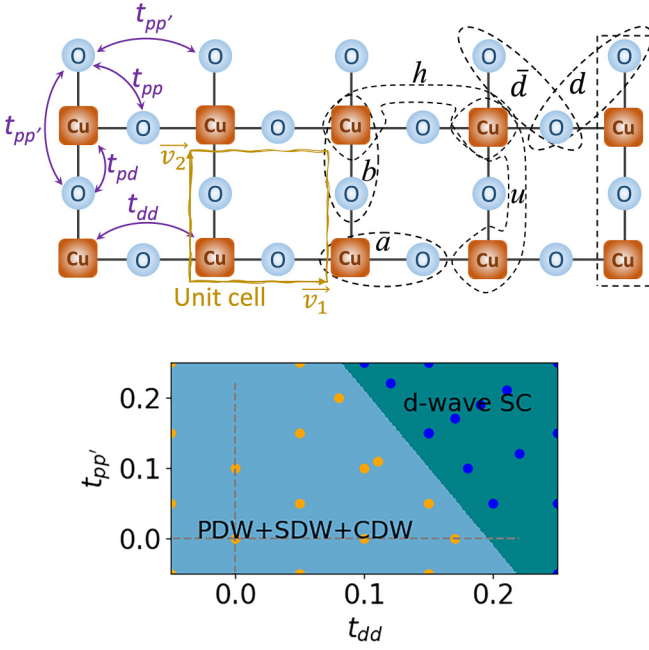
*Contact author: luhyang@stanford.edu

FIG. 1. Top: The three-band Hubbard model on a Lieb lattice. The hopping parameters are shown on the lattice. Several types of copper-copper bonds are marked in dashed lines. We add an additional column on the right end to facilitate convergence. Here, $\vec{v}_1$ and $\vec{v}_2$ are basis vectors in the unit cell. Bottom: Phase diagram as a function of t_{dd} and $t_{pp'}$. The region in orange represents the PDW+CDW+SDW phase, and the region in blue is the SC phase.

correlations and discuss how the hopping parameters affect the ground state properties; in Sec. IV, we present an analysis of down-folding the three-band Hubbard model to an effective t-t'-J-J' model using the exact diagonalization method; finally, in Sec. V, we summarize our results.

II. MODEL AND PHASE DIAGRAM

We use the density-matrix renormalization group (DMRG) method [39–41] based on the iTensor library [42,43] to study the ground state phase diagram of the three-band Hubbard model with further-neighbor hoppings on two-leg ($L_y = 2$) Lieb lattice cylinders with length up to $L_x = 64$. By keeping bond dimensions up to $m = 7000$, we make sure the truncation error remains in the order of 10^{-7} or below. The Lieb lattice we simulate is shown in the top panel of Fig. 1. The "squares" and "circles" represent copper and oxygen orbitals, respectively. We implement the periodic (open) boundary condition along the vertical (horizontal) direction.

We study the following model Hamiltonian in the hole language:

$$H = H_{tb} + H_{\text{int}} \qquad (1)$$

$$H_{tb} = -T^{pd} - T^{pp} - T^{dd} - T^{pp'}$$
$$+ \Delta_{pd} \sum_i n_i^p \qquad (2)$$

$$H_{\text{int}} = U_d \sum_i n_{\uparrow,i}^d n_{\downarrow,i}^d + U_p \sum_i n_{\uparrow,i}^p n_{\downarrow,i}^p, \qquad (3)$$

where the kinetic term is defined as $T^{\alpha\beta} = \sum_{i,j;\sigma} t_{\alpha\beta}(c_{i,\sigma}^{\alpha\dagger} c_{j,\sigma}^{\beta} + \text{H.c.})$, and α, β belongs to each kind of orbitals. We take into account four types of hopping terms in this model as shown in the top panel of Fig. 1: (1) t_{pd} between the adjacent oxygen and copper sites, (2) t_{pp} between the nearest p_x and p_y orbitals, (3) t_{dd} between copper sites in the adjacent unit cells, and (4) $t_{pp'}$ between the same type of oxygen sites in the adjacent cells. In this work, we keep $U_d = 8$, $U_p = 3$, $t_{pd} = 1$, $t_{pp} = 0.5$, and $\Delta_{pd} = 3$ [44–46] unless otherwise specified. t_{dd} and t'_{pp} are the tuning parameters. We follow the sign convention in Ref. [5], which is equivalent to the original Emery model by a gauge transformation.

We calculate the following correlation functions to study the ground state properties of the systems. These include the spin-spin correlation function

$$S(r) = \langle S_0^z S_r^z \rangle, \qquad (4)$$

the charge density-density fluctuation correlation function

$$D(r) = \langle n_0 n_r \rangle - \langle n_0 \rangle \langle n_r \rangle, \qquad (5)$$

the single-particle Green function

$$G(r) = \langle c_{\uparrow,0}^\dagger c_{\uparrow,r} \rangle, \qquad (6)$$

and the spin-singlet SC pair-pair correlation function

$$\Phi(r) = \langle \tilde{\Delta}_0^\dagger \tilde{\Delta}_r \rangle. \qquad (7)$$

Here, $\tilde{\Delta}^\dagger$ represents the spin-singlet Cooper pair creation operator between neighboring sites

$$\tilde{\Delta}_i^\dagger = \frac{1}{\sqrt{2}}(c_{i,\downarrow}^\dagger c_{i+1,\uparrow}^\dagger - c_{i,\uparrow}^\dagger c_{i+1,\downarrow}^\dagger). \qquad (8)$$

In the bottom panel of Fig. 1, we show the phase diagram as a function of t_{dd} and t'_{pp} at $\delta = 1/8$ hole doping concentration. When both hopping parameters are around zero, the system is in a Luttinger liquid phase with intertwined PDW, CDW, and SDW correlations. To find the strongest signal of the pairing order, we have computed the SC pairing correlations on different bonds (see Appendix B) and find that $\Phi_{hh}(r)$, i.e., the spin-singlet SC pairs on nearest copper sites along the x-direction, is the dominant SC component. By increasing both hopping coefficients to the positive values, the spin-singlet pairing correlations are further enhanced and the system eventually undergoes a quantum phase transition to a d-wave SC phase. The properties of this d-wave SC phase is consistent with that of a Luther-Emery liquid state with quasi-long-range SC and CDW correlations but short-range spin-spin correlation (see Appendix D). Different from the Luttinger liquid phase, the spin-singlet pairing correlation between adjacent copper sites along the y-direction $\Phi_{uu}(r)$ becomes dominant over all the other bonds here and exhibits a d-wave symmetry.

III. GROUND STATE CORRELATIONS

When t_{dd} and t'_{pp} are both small and positive, the ground state of the system is consistent with that of the Luttinger liquid phase with power-law single-particle, PDW, SDW, and CDW correlations. However, different from the single-band Hubbard model, the SC correlation (see the right panel of Fig. 9) in this case has a spatial oscillation with sign change
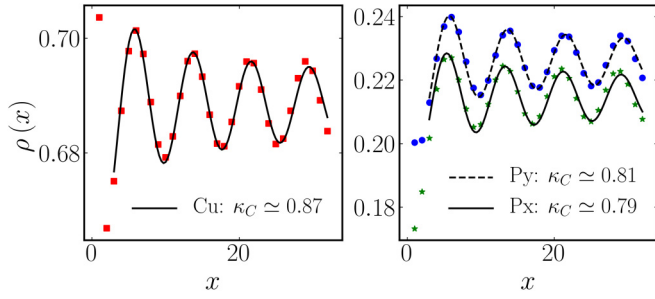
FIG. 2. Local density profiles for $t_{dd} = t'_{pp} = 0.2$. Left: Density distribution on copper orbital. Right: Density distribution on oxygen orbital. κ_C is the scaling exponent obtained by curve fitting.

(see Appendix C), which can be described by the following formula:

$$\langle \tilde{\Delta}_0^\dagger \tilde{\Delta}_r \rangle = \frac{A \cdot \cos(\omega r + \phi)}{r^{\kappa_{pdw}}} + \frac{B}{r^{\kappa_{sc}}}. \qquad (9)$$

If the value of $B \lesssim A$, the overall fluctuation has a spatial oscillation around zero, which suggests the presence of the PDW order. Our results are consistent with this, where we find that $A \approx 10B$ when $t_{dd} = t'_{pp} = 0$. For $t_{dd} = t'_{pp} = 0.2$, we find that $A \approx B/3$.

The charge density properties of the system can be described by the charge density profile $n_\alpha(x, y)$ and its rung average $\rho_\alpha(x) = \sum_{y=1}^{L_y} n_\alpha(x, y)/L_y$, where x denotes the position along the longer direction, y is the position along the shorter direction, and α represents each type of orbital. Consistent with previous studies [5,6], the spatial decay of the CDW correlation at long distance is dominated by a power law with an exponent κ_c with two ordering wavevectors $Q = 2\pi\delta$ and $2Q$ (see Fig. 10). The value of the exponent κ_c can be obtained by fitting the charge density oscillations $\rho(x)$ with a generalized Friedel oscillation formula induced by the open boundaries of the cylinder [5,47]

$$\rho(x) = \frac{A_Q * \cos(Qx + \phi_1)}{x^{\kappa_c/2}} + \frac{A_{2Q} * \cos(2Qx + \phi_2)}{x^{\kappa_c/2}} + n_0, \qquad (10)$$

where A_Q and A_{2Q} are the amplitudes, ϕ_1 and ϕ_2 are the phase shifts, and n_0 is the mean density. It has been shown that the $2Q$ charge order usually competes with the superconductivity [14,48], which is also consistent with our results. We will see that when the system enters the superconducting phase, the $2Q$ mode is suppressed.

By increasing the parameters to the larger positive values, the system enters a distinct d-wave SC phase with dominant power-law superconducting correlations but exponentially decaying single-particle and spin-spin correlations. In the d-wave SC phase, the short-ranged spin-spin correlation is mutually commensurate with the charge correlation at the wavevector Q, although both of them are incommensurate on the finite lattice with open boundaries in the longer direction.

Contrary to the Luttinger liquid phase with small further-neighbor electron hoppings, we find that in this d-wave SC phase, the coefficient B is greater than A. Moreover, the charge density modulation has only one characteristic wavevector Q (Fig. 2). The $2Q$ mode is suppressed while the SC order
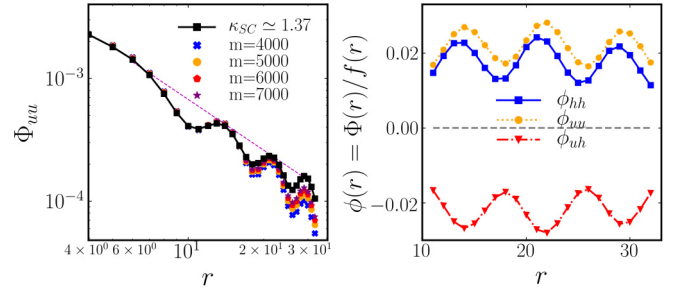

FIG. 3. Correlations for $t_{dd} = t'_{pp} = 0.2$. Left: Singlet pairing correlations on u bonds in log scale for different number of states m. The black curve with square symbols represents the result of a $m \to \infty$ extrapolation. Right: The normalized pairing correlations on $u - u$, $h - h$, and $u - h$ bonds, where the u, h bonds are shown in the lattice in Fig. 1. $f(r)$ is the envelope function.

is enhanced. The symmetry of the SC correlations can be determined by comparing the relative signs of the SC pair-pair correlations between different bonds. The right panel of Fig. 3 shows that the pairing correlations between u bonds display values in opposite sign with the correlations between u and h bonds (see Fig. 1 for the definition of the bonds). Besides, the multiplication of κ_c and κ_{sc} is close to 1. All of these suggest that the system is in a Luther-Emery phase, with a d-wave pairing symmetry, and these conclusions are not system dependent based on our study on ladders with different lengths (see Appendix E).

The preceding results show that the intercell hopping terms enhance the SC correlations while suppressing the spin-spin correlation. This is closely connected to the results of charge transfer energy, which also suggests that the density distribution is associated with the intertwined orders in the charge transfer insulators [49]. To understand how these two pictures reconcile, we study how the hopping terms affect the density distributions on each orbital. It is shown in other works [45,46] that for the undoped three-band Hubbard model, about 70% of the holes are on the copper sites. Upon (hole) doping, however, most of the doped holes will occupy the oxygen sites [49]. Interestingly, if we turn on the further-neighbor electron hoppings t_{dd} and t'_{pp}, we find that the effect of increasing t'_{pp} is equivalent to decreasing the effective Δ_{pd}, where the average copper density will decrease (see Appendix A). On the contrary, the influence of t_{dd} on density distribution is negligible.

As a complementary comparison, we have computed the SC pairing correlation for different charge transfer energies Δ_{pd} while all the other parameters remain the same. In Fig. 4, we show the SC pairing correlations for two representative cases in each of the two phases, where we find that for both phases, decreasing Δ_{pd} can enhance the SC pairing correlations.

IV. DOWN-FOLDING THE THREE-BAND HUBBARD MODEL TO AN EFFECTIVE t-t'-J-J' MODEL

The low-energy physics of the three-band Hubbard model (or CuO$_2$ plane) can be mapped to an effective t-t'-J-J' model in Eq. (11). Following the prescription in Refs. [18–20], we
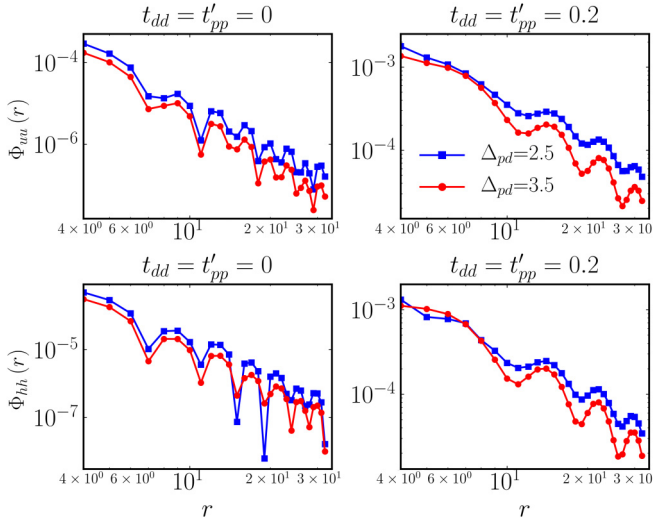
FIG. 4. Comparison of singlet pairing correlations with different values of charge transfer energy in each of the PDW + CDW + SDW and SC phases.
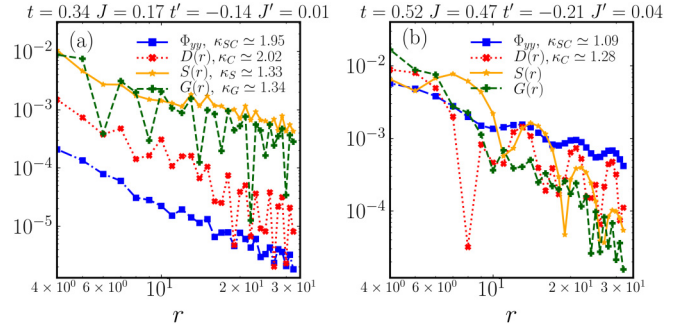

FIG. 5. Ground state correlations of the t-t'-J-J' model. (a) The results for $t = 0.34$, $t' = -0.14$, $J = 0.17$, $J' = 0.01$. The corresponding three-band Hubbard model is in the LL phase. (b) The results for $t = 0.52$, $t' = -0.21$, $J = 0.47$, $J' = 0.04$. The corresponding three-band Hubbard model is in the SC phase.
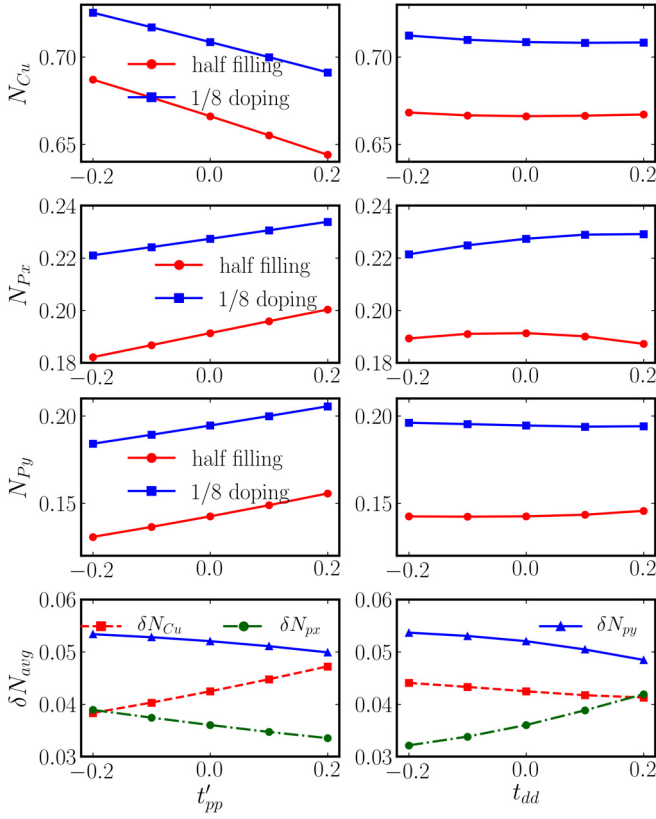
present the down-folding for the three-band Hubbard model with further-neighbor hopping terms. In this scheme, we consider two types of small clusters: the Cu_2O_7 cluster with two unit cells aligned, and the Cu_2O_8 cluster with the two unit cells along the diagonal direction. Specifically, the hopping parameter t (t') is determine by the spin-singlet and triplet energy splitting of a Cu_2O_7 (Cu_2O_8) cluster; J (J') is determined by the energy difference between bonding and antibonding states of a Cu_2O_7 (Cu_2O_8) cluster. The results are shown in Table I. When the three-band Hubbard model is in the d-wave SC phase, we find in the effective model that the hoppings to both the nearest- (t) and next-nearest (t') neighbors are enhanced, as well as the spin exchange coupling J. The strengthening of the hybridization between orbitals makes the pairing orders more favorable.

$$H_{t-t'-J-J'} = -t \sum_{\langle i,j \rangle \sigma} (c_{i,\sigma}^\dagger c_{j,\sigma} + \text{H.c.})$$

$$- t' \sum_{\langle\langle i,j \rangle\rangle \sigma} (c_{i,\sigma}^\dagger c_{j,\sigma} + \text{H.c.})$$

$$+ J \sum_{\langle i,j \rangle \sigma} \left(\vec{S}_i \cdot \vec{S}_j - \frac{1}{4} n_i n_j \right)$$

$$+ J' \sum_{\langle\langle i,j \rangle\rangle} \left(\vec{S}_i \cdot \vec{S}_j - \frac{1}{4} n_i n_j \right) \quad (11)$$

TABLE I. Coefficients of the effective t-t'-J-J' model. There is an overall minus sign before each hopping coefficient.

t_{dd}	t'_{pp}	Cu_2O_7		Cu_2O_8	
		t	J	t'	J'
0	0	0.34	0.17	–0.14	0.01
0	0.25	0.45	0.27	–0.21	0.04
0.25	0	0.41	0.34	–0.14	0.01
0.25	0.25	0.52	0.47	–0.21	0.04

To further support this argument, we have also calculated the ground state properties of the t-t'-J-J' model on an $N = 64 \times 2$ ladder with DMRG, using the parameters listed in Table I. We choose two representative sets of parameters in the first and last rows of the table to implement the calculations. The corresponding three-band Hubbard models of these two data points are in the Luttinger liquid phase and d-wave SC phase, respectively. The results are presented in Fig. 5. We can see in the left panel that all the correlations decay as a power law, with dominant single-particle and spin correlations. However in the right panel, the SC pairing and CDW correlations become dominant while the spin and single-particle correlations are short ranged, which decay exponentially. Similar to the three-band Hubbard model, the pairing symmetry of the SC correlations is also d-wave in this case.

V. CONCLUSIONS

To summarize, we have studied the ground state properties of the lightly doped three-band Hubbard model with longer-range hopping terms on two-leg cylinders. By tuning these hopping coefficients positively, we observed a quantum phase transition from a Luttinger liquid phase characterized by intertwined PDW, CDW, and SDW correlations to a d-wave SC phase (i.e., Luther-Emery phase). Through this transition, the pairing order intensifies, changing from a mixed SC and PDW order to a predominantly d-wave symmetry SC order. This transition is underlined by modifications in the band structure and density distributions stemming from the tuning of hopping parameters. Our computational analyses pinpointed an intriguing correlation: the increase in the t'_{pp} parameter mimics the effect of a reduced effective charge transfer energy, Δ_{pd}.
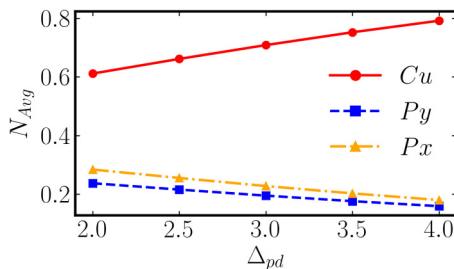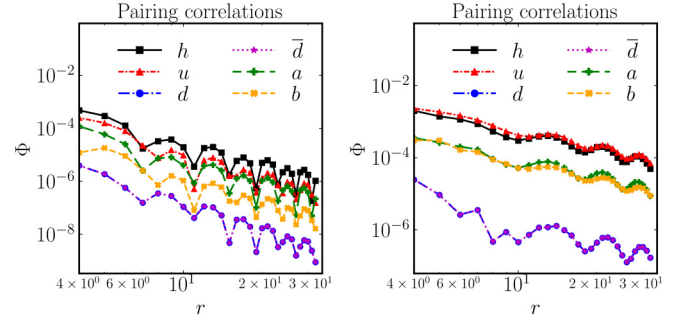
By down-folding the three-band Hubbard model to the effective t-t'-J-J' model, we observed an increase of both the nearest- and second-neighbor hopping parameters and the ratio of J/t, when entering the Luther-Emery phase. This finding sheds light on the question as to "why the lightly doped three-band Hubbard ladder behaves as a Luttinger liquid but not the Luther-Emery liquid, as the single-band Hubbard model does." From our small cluster study, we found that although these two models were closely related, the parameters of the original three-band Hubbard model did not have

FIG. 6. Number density measurements on Cu, O_x, and O_y sites.

FIG. 8. Left: Comparison of singlet pairing correlations on different bonds for $t_{dd} = t'_{pp} = 0$. Right: Comparison of singlet pairing correlations on different bonds for $t_{dd} = t'_{pp} = 0.2$. The u, h, a, b, d, and $\bar{d}$ bonds are shown in the lattice in Fig. 1.
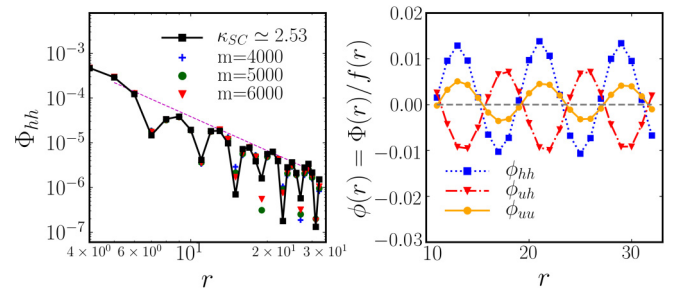
for enhancing or in some instances even inducing the PDW order and superconductivity [5,6,50–52].

APPENDIX A: EFFECTS OF HOPPING PARAMETERS AND CHARGE TRANSFER ENERGY ON DENSITY DISTRIBUTION

To demonstrate how the hopping coefficients affect the number density, we compute the average density on copper and oxygen sites for systems with length $Lx = 48$ for two cases: (1) half filling and (2) 1/8 hole doping. Figure 6 shows the average local densities on Cu, O_x, and O_y sites with different values of intra-orbital hoppings. In both of the half filling and the hole-doped regimes, the density on copper sites mainly depends on the values of t'_{pp} and keeps nearly unchanged with t_{dd}. When t'_{pp} is increasing, the occupation

a strong enough hybridization between orbitals. However, by introducing longer-range hopping terms, the Luther-Emery phase emerges in the vicinity of the Luttinger liquid phase.

In this study, we have examined the effect of further-neighbor particle hopping terms on the ground state properties of the three-band Hubbard model on two-leg cylinders. It is worth noting that the recovery of the Luther-Emery phase on the three-band Hubbard model can also be achieved by introducing long-range Coulomb interactions [6]. An intriguing avenue for future research would be to ascertain whether this influence persists in wider systems and at higher doping levels. A comprehensive understanding would also necessitate the exploration of the combined effects of further-neighbor hopping and long-range Coulomb interactions, for which previous studies have demonstrated that the latter one is crucial

FIG. 7. Average number density as a function of Δ_{pd}. Computed by DMRG for system size $Nx = 48$ with 1/8 doping.

FIG. 9. Correlations for $t_{dd} = t'_{pp} = 0$. Left: Singlet pairing correlations on h bonds in log scale; the black curve with square symbols represents the result of extrapolation to $m \to \infty$. Right: The normalized pairing correlations on $h - h$, $u - u$, and $u - h$ bonds. $f(r)$ is the envelope function.
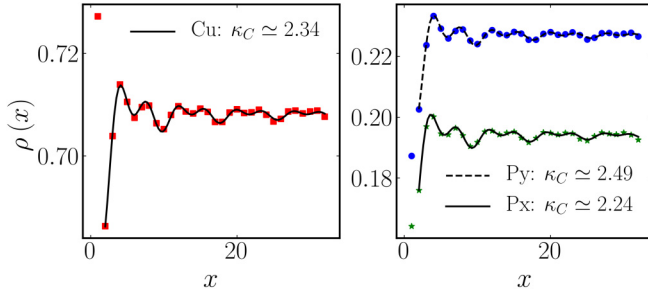
FIG. 10. Local density profiles for $t_{dd} = t'_{pp} = 0$. Left: Density distribution on copper orbital. Right: Density distribution on oxygen orbital. κ_C is the scaling exponent obtained by curve fitting.

number on Cu sites decreases and more holes go to oxygen sites, which is similar to the effect of decreasing the charge transfer energy Δ_{pd} (Fig. 7).

Nevertheless, the doped holes (the increase of the hole density upon doping) have both t_{dd} and t'_{pp} dependencies. With the increase of t'_{pp}, the doped holes on both O_x and O_y decrease. With the increase of t_{dd}, the doped holes on O_x and O_y have opposite trends and the number of doped holes on copper sites decreases.

APPENDIX B: COMPARISON OF THE PAIRING ORDERS ON DIFFERENT BONDS

In Fig. 8, we show the pairing correlations on all types of bonds illustrated in the top panel of the schematic in Fig. 1. When the system is in the PDW phase, the PDW order on the h bonds is slightly stronger than all the others, although all of the pairing orders are quasi-long ranged. However, in the d-wave SC phase, the SC order on u and h bonds are dominant, and are stronger than the others by a few orders of magnitude.

APPENDIX C: GROUND STATE CORRELATIONS IN THE LL PHASE

We choose one representative data point in the LL phase and present the ground state properties. For the case $t_{dd} = t'_{pp} = 0$, we show the pairing correlations in Fig. 9. The pairing order has a spatial oscillation with a vanishing average and exhibits a d-wave symmetry. Figure 10 shows the local density profile and the decaying exponent obtained by curve fitting with Eq. (10).
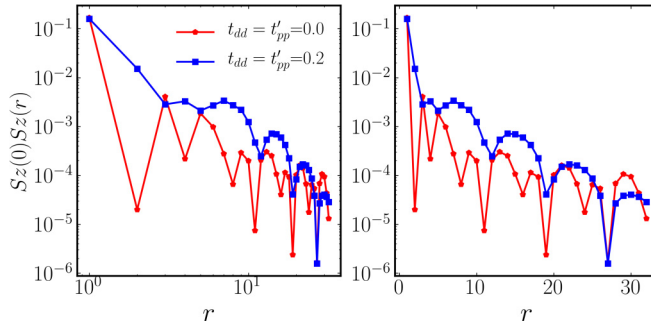

FIG. 11. Spin-spin correlations for $t_{dd} = t'_{pp} = 0$ and $t_{dd} = t'_{pp} = 0.2$. Left: Log-log scale. Right: Semi-log scale.
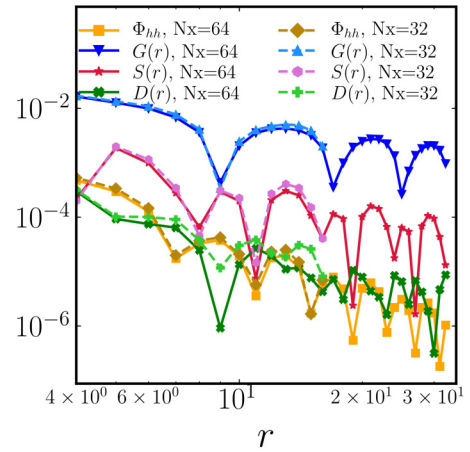

FIG. 12. Comparison of the correlations with different system sizes for $t_{dd} = t'_{pp} = 0$.

APPENDIX D: SPIN-SPIN CORRELATIONS IN EACH OF THE TWO PHASES

To address the magnetic properties of the system in different phases, we compute the spin-spin correlations defined in Eq. (4), and the results are presented in Fig. 11. Two representative cases are chosen to present in this figure. The log-log and semi-log plots clearly reveal the different scaling behaviors. The $S(r)$ in the PDW+SDW+CDW phase exhibits a power-law decay (for $t_{dd} = t'_{pp} = 0$), which appears as a linear curve in the log-log plot but a nonlinear curve in the semi-log plot. In contrast, the $S(r)$ in the SC phase (with $t_{dd} = t'_{pp} = 0.2$) exhibits an exponential decay, which appears as a nonlinear curve in the log-log plot but a linear curve in the semi-log plot, indicating that the spin sector is gapped.

APPENDIX E: COMPARISON OF DIFFERENT SYSTEM SIZES

We have computed the spin-spin, density-density, single-particle, and pairing correlations for systems of size 64×2
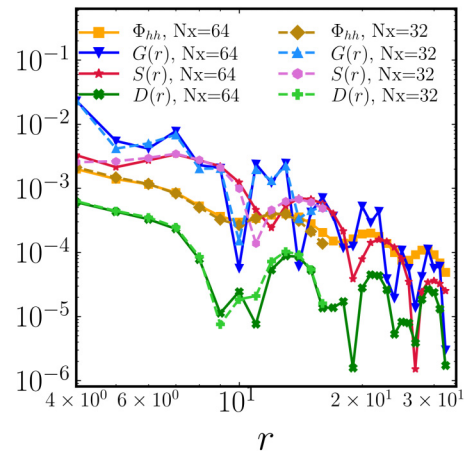

FIG. 13. Comparison of the correlations with different system sizes for $t_{dd} = t'_{pp} = 0.2$.

and 32×2, and present the results in Figs. 12 and 13. Both of these figures demonstrate that the trends and decaying behaviors of varied correlations are independent of system size across both phases.

[1] V. J. Emery, Theory of high-T_c superconductivity in oxides, Phys. Rev. Lett. **58**, 2794 (1987).

[2] V. J. Emery and G. Reiter, Mechanism for high-temperature superconductivity, Phys. Rev. B **38**, 4547 (1988).

[3] M. Hirayama, Y. Yamaji, T. Misawa, and M. Imada, *Ab initio* effective Hamiltonians for cuprate superconductors, Phys. Rev. B **98**, 134501 (2018).

[4] M. Hirayama, T. Misawa, T. Ohgoe, Y. Yamaji, and M. Imada, Effective Hamiltonian for cuprate superconductors derived from multiscale *ab initio* scheme with level renormalization, Phys. Rev. B **99**, 245155 (2019).

[5] H.-C. Jiang, Pair density wave in the doped three-band Hubbard model on two-leg square cylinders, Phys. Rev. B **107**, 214504 (2023).

[6] H.-C. Jiang and T. P. Devereaux, Pair density wave and superconductivity in a kinetically frustrated doped Emery model on a square lattice, arXiv:2309.11786.

[7] E. Berg, E. Fradkin, and S. A. Kivelson, Pair-density-wave correlations in the Kondo-Heisenberg model, Phys. Rev. Lett. **105**, 146403 (2010).

[8] J. Almeida, G. Roux, and D. Poilblanc, Pair density waves in coupled doped two-leg ladders, Phys. Rev. B **82**, 041102(R) (2010).

[9] A. Jaefari and E. Fradkin, Pair-density-wave superconducting order in two-leg ladders, Phys. Rev. B **85**, 035104 (2012).

[10] M. Zegrodnik and J. Spałek, Incorporation of charge- and pair-density-wave states into the one-band model of d-wave superconductivity, Phys. Rev. B **98**, 155144 (2018).

[11] X. Y. Xu, K. T. Law, and P. A. Lee, Pair density wave in the doped $t-j$ model with ring exchange on a triangular lattice, Phys. Rev. Lett. **122**, 167001 (2019).

[12] J. May-Mann, R. Levy, R. Soto-Garrido, G. Y. Cho, B. K. Clark, and E. Fradkin, Topology and the one-dimensional Kondo-Heisenberg model, Phys. Rev. B **101**, 165133 (2020).

[13] Y.-H. Zhang and A. Vishwanath, Pair-density-wave superconductor from doping Haldane chain and rung-singlet ladder, Phys. Rev. B **106**, 045103 (2022).

[14] D. P. Arovas, E. Berg, S. A. Kivelson, and S. Raghu, The Hubbard model, Annu. Rev. Condens. Matter Phys. **13**, 239 (2022).

[15] M. Qin, T. Schäfer, S. Andergassen, P. Corboz, and E. Gull, The Hubbard model: A computational perspective, Annu. Rev. Condens. Matter Phys. **13**, 275 (2022).

[16] F. C. Zhang and T. M. Rice, Effective Hamiltonian for the superconducting Cu oxides, Phys. Rev. B **37**, 3759 (1988).

[17] S. Jiang, D. J. Scalapino, and S. R. White, A single-band model with enhanced pairing from DMRG-based downfolding of the three-band Hubbard model, Phys. Rev. B **108**, L161111 (2023).

[18] H. Eskes, G. Sawatzky, and L. Feiner, Effective transfer for singlets formed by hole doping in the high-T_c superconductors, Phys. C: Supercond. Appl. **160**, 424 (1989).

[19] H. Eskes and G. A. Sawatzky, Single-, triple-, or multiple-band Hubbard models, Phys. Rev. B **44**, 9656 (1991).

[20] H. Eskes and G. A. Sawatzky, Doping dependence of high-energy spectral weights for the high-T_c cuprates, Phys. Rev. B **43**, 119 (1991).

[21] L. F. Feiner, J. H. Jefferson, and R. Raimondi, Effective single-band models for the high-T_c cuprates. I. Coulomb interactions, Phys. Rev. B **53**, 8751 (1996).

[22] R. Raimondi, J. H. Jefferson, and L. F. Feiner, Effective single-band models for the high-T_c cuprates. II. Role of apical oxygen, Phys. Rev. B **53**, 8774 (1996).

[23] V. I. Belinicher and A. L. Chernyshev, Reduction of a three-band model for copper oxides to a single-band generalized t-J model, Phys. Rev. B **47**, 390 (1993).

[24] E. W. Huang, C. B. Mendl, S. Liu, S. Johnston, H.-C. Jiang, B. Moritz, and T. P. Devereaux, Numerical evidence of fluctuating stripes in the normal state of high-T_c cuprate superconductors, Science **358**, 1161 (2017).

[25] E. W. Huang, C. B. Mendl, H.-C. Jiang, B. Moritz, and T. P. Devereaux, Stripe order from the perspective of the Hubbard model, npj Quantum Mater. **3**, 22 (2018).

[26] J. E. Hirsch, Two-dimensional Hubbard model: Numerical simulation study, Phys. Rev. B **31**, 4403 (1985).

[27] H. Yokoyama, M. Ogata, and Y. Tanaka, Mott transitions and d-wave superconductivity in half-filled-band Hubbard model on square lattice with geometric frustration, J. Phys. Soc. Jpn. **75**, 114706 (2006).

[28] G. Dopf, A. Muramatsu, and W. Hanke, Three-band Hubbard model: A Monte Carlo study, Phys. Rev. B **41**, 9264 (1990).

[29] T. Yanagisawa, S. Koike, and K. Yamaji, Ground state of the three-band Hubbard model, Phys. Rev. B **64**, 184509 (2001).

[30] Y. Shen, G.-M. Zhang, and M. Qin, Reexamining doped two-legged Hubbard ladders, Phys. Rev. B **108**, 165113 (2023).

[31] H.-C. Jiang, Z.-Y. Weng, and S. A. Kivelson, Superconductivity in the doped $t-J$ model: Results for four-leg cylinders, Phys. Rev. B **98**, 140505(R) (2018).

[32] J.-P. Song, S. Mazumdar, and R. T. Clay, Absence of Luther-Emery superconducting phase in the three-band model for cuprate ladders, Phys. Rev. B **104**, 104504 (2021).

[33] M. Aichhorn, E. Arrigoni, M. Potthoff, and W. Hanke, Antiferromagnetic to superconducting phase transition in the hole- and electron-doped Hubbard model at zero temperature, Phys. Rev. B **74**, 024508 (2006).

[34] B. Ponsioen, S. S. Chung, and P. Corboz, Period 4 stripe in the extended two-dimensional Hubbard model, Phys. Rev. B **100**, 195141 (2019).

[35] H.-C. Jiang and T. P. Devereaux, Superconductivity in the doped Hubbard model and its interplay with next-nearest hopping t', Science **365**, 1424 (2019).

[36] Y.-F. Jiang, J. Zaanen, T. P. Devereaux, and H.-C. Jiang, Ground state phase diagram of the doped Hubbard model on the four-leg cylinder, Phys. Rev. Res. **2**, 033073 (2020).

[37] S. Jiang, D. J. Scalapino, and S. R. White, Ground state phase diagram of the t-t'-J model, Proc. Natl. Acad. Sci. USA **118**, e2109978118 (2021).

[38] Y.-F. Jiang, T. P. Devereaux, and H.-C. Jiang, Ground state phase diagram and superconductivity of the doped Hubbard model on six-leg square cylinders, arXiv:2303.15541.

[39] S. R. White, Density matrix formulation for quantum renormalization groups, Phys. Rev. Lett. **69**, 2863 (1992).

[40] S. R. White, Density-matrix algorithms for quantum renormalization groups, Phys. Rev. B **48**, 10345 (1993).

[41] S. Östlund and S. Rommer, Thermodynamic limit of density matrix renormalization, Phys. Rev. Lett. **75**, 3537 (1995).

[42] M. Fishman, S. R. White, and E. M. Stoudenmire, The ITensor software library for tensor network calculations, SciPost Phys. Codebases 4, (2022).

[43] M. Fishman, S. R. White, and E. M. Stoudenmire, Codebase release 0.3 for ITensor, SciPost Phys. Codebases 4-r0.3, (2022).

[44] M. S. Hybertsen, M. Schlüter, and N. E. Christensen, Calculation of Coulomb-interaction parameters for La_2CuO_4 using a constrained-density-functional approach, Phys. Rev. B **39**, 9028 (1989).

[45] S. Nishimoto, E. Jeckelmann, and D. J. Scalapino, Differences between hole and electron doping of a two-leg CuO ladder, Phys. Rev. B **66**, 245109 (2002).

[46] S. R. White and D. J. Scalapino, Doping asymmetry and striping in a three-orbital CuO_2 Hubbard model, Phys. Rev. B **92**, 205112 (2015).

[47] S. R. White, I. Affleck, and D. J. Scalapino, Friedel oscillations and charge density waves in chains and ladders, Phys. Rev. B **65**, 165122 (2002).

[48] D. F. Agterberg and J. Garaud, Checkerboard order in vortex cores from pair-density-wave superconductivity, Phys. Rev. B **91**, 104512 (2015).

[49] R. T. Scalettar, D. J. Scalapino, R. L. Sugar, and S. R. White, Antiferromagnetic, charge-transfer, and pairing correlations in the three-band Hubbard model, Phys. Rev. B **44**, 770 (1991).

[50] Z. Chen, Y. Wang, S. N. Rebec, T. Jia, M. Hashimoto, D. Lu, B. Moritz, R. G. Moore, T. P. Devereaux, and Z.-X. Shen, Anomalously strong near-neighbor attraction in doped 1D cuprate chains, Science **373**, 1235 (2021).

[51] D.-W. Qu, B.-B. Chen, H.-C. Jiang, Y. Wang, and W. Li, Spin-triplet pairing induced by near-neighbor attraction in the extended Hubbard model for cuprate chain, Commun. Phys. **5**, 257 (2022).

[52] C. Peng, Y. Wang, J. Wen, Y. S. Lee, T. P. Devereaux, and H.-C. Jiang, Enhanced superconductivity by near-neighbor attraction in the doped extended Hubbard model, Phys. Rev. B **107**, L201102 (2023).